

Calibration of *MAT_258 with a Lode dependent fracture surface and its application in bending of high-strength steel

J.K. Holmen^{1,2}, J. Johnsen^{1,2}, D. Morin^{2,3}, T. Børvik^{2,3}, M. Langseth^{2,3}

¹Enodo AS, Trondheim, Norway (mail@enodo.no)

²Structural Impact Laboratory (SIMLab), Department of Structural Engineering, Norwegian University of Science and Technology (NTNU), Trondheim, Norway

³Centre for Advanced Structural Analysis (SFI CASA), Department of Structural Engineering, NTNU, Trondheim, Norway

Abstract

MAT_258** (MAT_NON_QUADRATIC_FAILURE**) is a through-thickness failure regularization model for shells in LS-DYNA. In this model the failure indicator is computed as a function of both the size of the element and its bending-to-membrane loading ratio. The constitutive behavior and fracture surface in ***MAT_258** are represented by well-known analytical expressions which simplify calibration. We present the calibration process for ***MAT_258** with a three-parameter Extended Cockcroft-Latham fracture surface for the high strength steel Docol 1500M. The material card is applied in shell element simulations of three-point bend tests.

1 Introduction

It is challenging to accurately predict material fracture with shell elements. Due to computational limitations, the element size can sometimes be too large to sufficiently describe the deformed geometry. Behavior after diffuse necking is an example of an instance where coarsely meshed shell elements struggle to capture the correct behavior and where changes in the element size might alter the simulation result [1]. After subsequent local necking the material develops a three-dimensional stress state which leads to even stronger element size sensitivity. Another complicating matter is that plates that are subjected to pure bending do not suffer from local necking and the ductility can therefore be higher in bending than in membrane dominated loading.

Several approaches are used to improve the way shell elements predict ductile fracture. Pack and Mohr [2] developed a method where fracture both before and after necking can be modeled with shell elements, while Andrade et al. [3] provides a thorough description of the flexible GISSMO [4] framework for coupled damage and fracture which is available as ***MAT_ADD_DAMAGE_GISSMO** in LS-DYNA.

Costas et al. [5] first presented the theoretical background and the through-thickness regularization approach (TTR) which later was implemented in LS-DYNA as ***MAT_258**. The model works with separate fracture surfaces for bending dominated loads and membrane dominated loads. Failure under membrane loads is regularized with respect to element size to account for the fact that steep strain gradients cannot be resolved in large shells. While the simplest form of ***MAT_258** model has been showcased at previous LS-DYNA conferences [6,7], the current work uses a more elaborate fracture surface where the Lode dependence of fracture has been controlled [8]. This is done through the Extended Cockcroft-Latham (ECL) fracture criterion that was first presented by Gruben et al. [9]. Compared to the original Cockcroft-Latham (CL) fracture criterion, ECL improves the description of shear dominated and biaxial stress states [10]. Three material tests are required for a complete calibration.

All the simulations presented in this study are conducted with LS-DYNA Version MPP_DP_R9.3.0.

2 Model description

MAT_258** (MAT_NON_QUADRATIC_FAILURE**) features an isotropic elastic-viscoplastic strength model with a non-quadratic yield surface and an uncoupled damage indicator. Strain rate sensitivity following a modified Johnson-Cook approach [11], originally implemented into LS-DYNA as ***MAT_107** (***MAT_MODIFIED_JOHNSON_COOK**), can be used in the most recent versions of LS-DYNA.

Strength and hardening are governed by a three-term Voce work hardening rule

$$\sigma_Y = \sigma_0 + \sum_{i=1}^3 Q_i \left(1 - \exp\left(-\frac{\theta_i}{Q_i} \bar{\epsilon}^p\right) \right) \quad (1)$$

where σ_0 is the initial yield stress, θ_i and Q_i control the work hardening, and $\bar{\epsilon}^p$ is the equivalent plastic strain. The parameters σ_0 , θ_i , and Q_i can be determined from a uniaxial tension test.

Failure in the model is evaluated as a function of two main parts:

1. An uncoupled Extended Cockcroft-Latham (ECL) fracture criterion that is dependent on the stress triaxiality ratio and Lode parameter.
2. A regularization procedure for the failure strain that accounts for the element size and deformation mode.

The ECL fracture criterion [9] is a function of the equivalent stress $\bar{\sigma}$, the major principal stress σ_1 , and the minor principal stress σ_3 as

$$\dot{D} = \frac{\bar{\sigma}}{W_C} \left\langle \phi \frac{\sigma_1}{\bar{\sigma}} + (1 - \phi) \left(\frac{\sigma_1 - \sigma_3}{\bar{\sigma}} \right) \right\rangle^\gamma \bar{\epsilon}^p \quad (2)$$

where W_C is the Cockcroft-Latham (CL) failure parameter that controls the overall ductility while ϕ and γ control the shape of the fracture surface. In essence, damage is driven by the plastic strain amplified by a stress state dependent factor. Note the Macaulay brackets ($\langle x \rangle = \max(0, x)$) that prevents the failure indicator from growing under compression dominated stress states.

Figure 1 shows how the three model parameters W_C , ϕ , and γ affect the shape of the plane stress fracture surface. W_C controls the overall ductility of the material, ϕ lowers the strain to failure for low stress triaxiality ratios, while γ lowers the strain to failure for biaxial stress states. In this model, the strain to failure is always equal for uniaxial tension and equibiaxial tension.

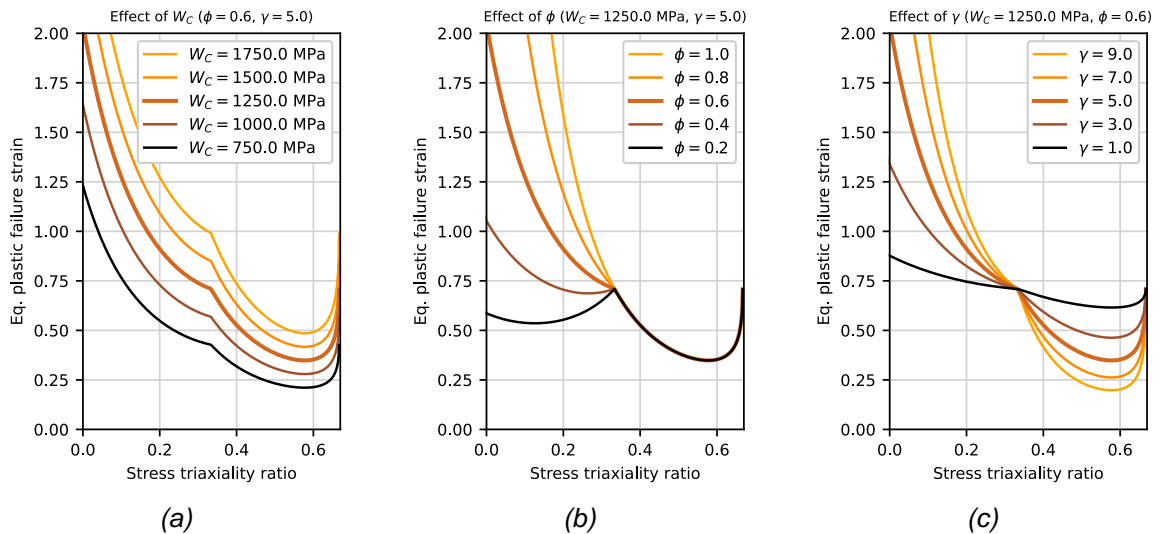


Figure 1: Effect of model parameters on the shape of the fracture surface. (a) W_C , (b) ϕ , and (c) γ .

During the simulation, the CL failure parameter that is used by LS-DYNA is determined by the following equation

$$W_c = \Omega W_c^b + (1 - \Omega) W_c^m \quad (3)$$

Here, W_c^b is the CL failure parameter in pure bending, W_c^m is the CL failure parameter in pure membrane loading, and Ω is the bending indicator which is 0 for pure membrane loading and 1 for pure bending. The bending indicator is calculated by the material subroutine based on the through-thickness plastic strains on the upper (ε_{33}^{p+}) and lower (ε_{33}^{p-}) side of the shell element as follows

$$\Omega = \frac{1}{2} \frac{|\varepsilon_{33}^{p+} - \varepsilon_{33}^{p-}|}{\max(|\varepsilon_{33}^{p+}|, |\varepsilon_{33}^{p-}|)} \quad (4)$$

The CL parameter in pure bending (W_c^b) is constant in the entire model throughout the simulation while the CL parameter in pure membrane loading (W_c^m) is a function of the element size:

$$W_c^m = W_c^l + (W_c^s - W_c^l) \exp\left(-c \left(\frac{l_e}{t_e} - 1\right)\right) \quad (5)$$

where W_c^l , W_c^s , and c are model parameters that must be calibrated while l_e and t_e are the characteristic side-length and thickness of each shell element. As will be shown later, W_c^s corresponds to W_c^m at $l_e/t_e = 1$ while W_c^l corresponds to the horizontal asymptote of Eq. (5) when $l_e/t_e \rightarrow \infty$.

3 Material tests

A 1 mm thick Docol 1500M steel plate delivered by SSAB was used in this study. It is a cold rolled martensitic steel commonly used for side impact beams, bumpers, and other structural components in cars. Three different specimen geometries were used for calibration of the material model:

- Uniaxial tension test (UT) shown in Figure 2(a). Used to calibrate the hardening curve in addition to the fracture surface. Initial stress triaxiality ratio ≈ 0.33 . Lode parameter ≈ -1.0 .
- Notched tension test (NT) shown in Figure 2(b). Used to calibrate the fracture surface. Initial stress triaxiality ratio ≈ 0.50 . Lode parameter ≈ 0.0 .
- In-plane single shear test (ISS) shown in Figure 2(c). Used to calibrate the fracture surface. Initial triaxiality ratio ≈ 0.0 , Lode parameter ≈ 0.0 .

All the tests were conducted in an Instron 5982 (100 kN) test machine and monitored by a Basler acA4112-30 μ m camera at an acquisition rate of 1 fps. 2D-DIC applying the DIC-code eCorr [12] was used to evaluate the displacement field on the surface of the samples. The crosshead velocity of the test machine was adjusted so that the initial strain rate was around 0.0005 1/s in the UT and NT tests, while it was 0.001 1/s in the ISS test. The longitudinal direction of the specimens was oriented along the rolling direction of the plate.

Figure 3 shows representative results from the material tests. The force was measured by the load cell in the test machine and normalized with respect to the initial area of the gauge. The elongation was extracted from the images using 2D-DIC. A 15 mm virtual extensometer was used in all the tests. The elongation was normalized with respect to the initial extensometer length. Obviously, for the UT test, Figure 3 shows the engineering stress-strain curve.

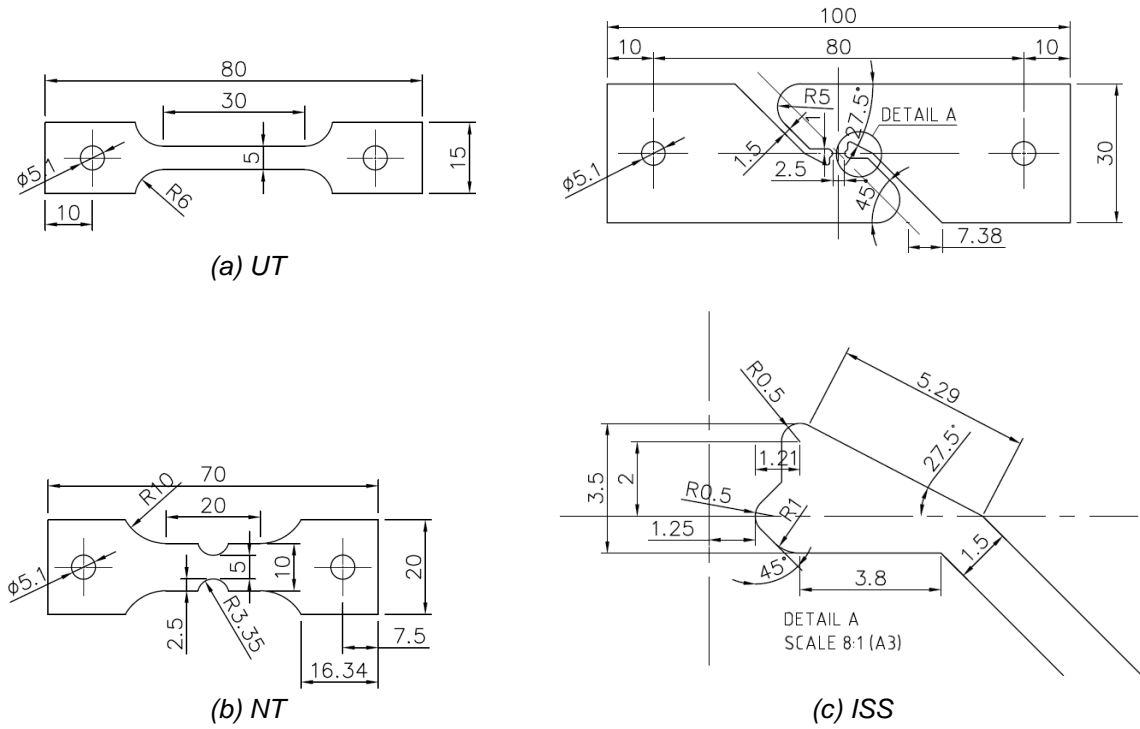


Figure 2: Test specimen geometries. (a) Uniaxial tension (UT), (b) notched tension (NT), and (c) in-plane single shear (ISS).

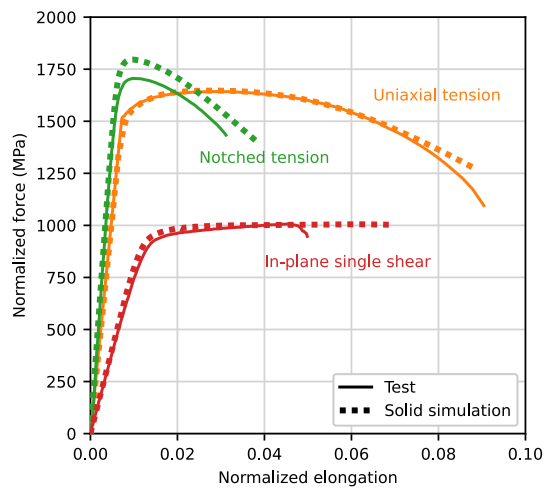


Figure 3: Results from material tests compared to the solid element simulations. The extensometer length was 15 mm in all tests. The force was normalized by the initial area of the cross section.

4 Calibration of the material model

The material model was calibrated using solid element simulations of the material tests. Figure 4 shows the undeformed models. Three symmetry planes were employed for the UT and NT tests. For the ISS test the only symmetry plane was the midplane of the plate. We used elements with side lengths of about 0.17 mm in the gauge area. This corresponds to 6 solid elements over the total thickness.

To calibrate the strength and hardening curve in `*MAT_258` we used LS-OPT. Sequential simulations on the UT test shown in Figure 4(a) were conducted to optimize the parameters in Eq. (1). Figure 5(a) shows the result. Figure 3 shows that the engineering stress-strain curve is close to the experimental curve. A slight overshoot at the tail end of the curve may be attributed to the constraints imposed by the symmetry planes or to the size of the elements.

We also used LS-OPT to calibrate W_c , ϕ , and γ in the ECL failure criterion. The optimized fracture surface is shown in Figure 5(b). Using the optimized hardening curve, we extracted σ_1 , σ_3 , $\bar{\sigma}$, and $\bar{\epsilon}^p$ from the critical element in each of the models in Figure 4. For UT and NT, the centermost element was chosen, and for ISS the critical element was the surface of the specimen, two element rows from the edge of the gauge. We then optimize W_c , ϕ , and γ in LS-OPT and Python by integrating Eq. (2) to find the values that make the failure occur as close as possible to the experiments. No sequential simulations are necessary with this calibration approach.

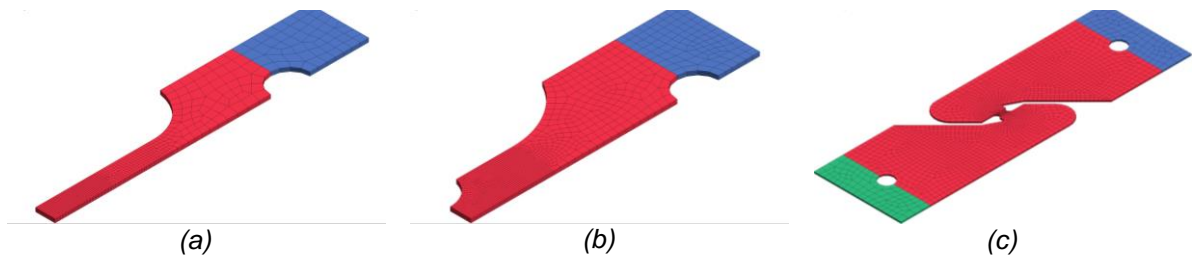


Figure 4: Simulation models used for calibration. (a) UT with three symmetry planes, (b) NT with three symmetry planes, and (c) ISS with one symmetry plane.

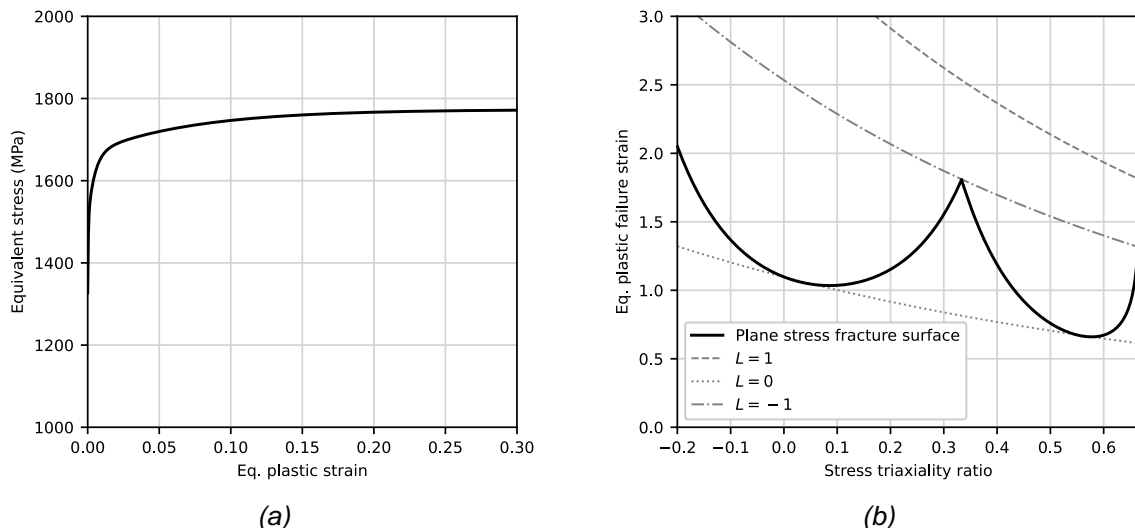


Figure 5: (a) Equivalent stress-strain curve. (b) Calibrated ECL plane stress fracture surface.

Single element models with boundary conditions extracted from the DIC analysis of the UT specimen were run to determine W_C^l , W_C^s , and c . Details regarding this procedure can be found in Costas et al. [5] and Holmen et al. [6]. Figure 6(a) shows the value of W_C^m determined by Eq. (5) for pure membrane loading. The failure parameter decreases as the element size increases to make up for the fact that the shell elements cannot resolve the strain and stress fields with sufficient accuracy. Figure 6(b) shows how the presence of bending increases the fracture parameter. For $\Omega = 1$ the fracture surface reverts to the surface for solid elements in Figure 5(b).

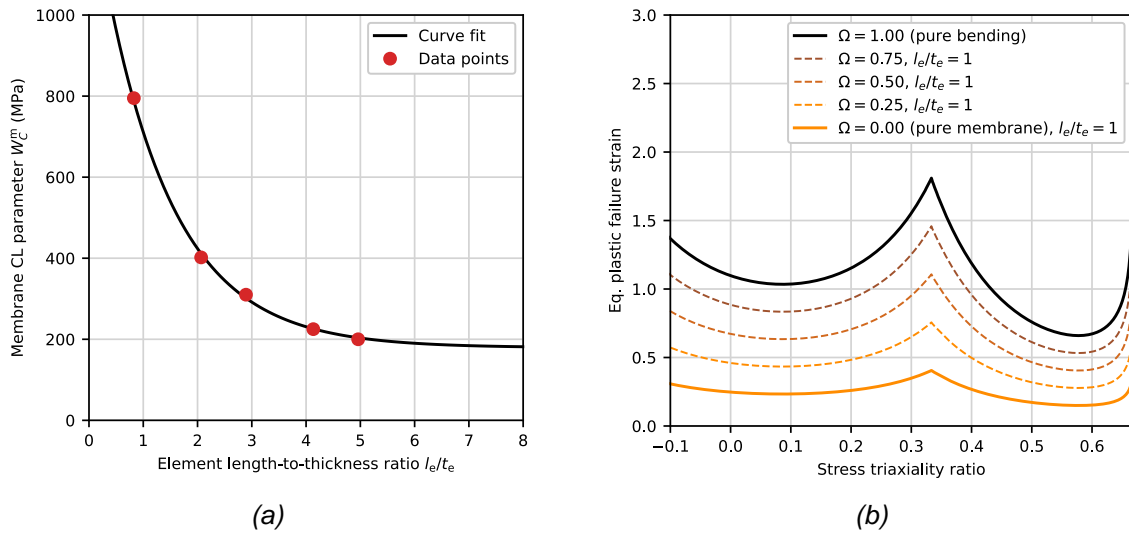


Figure 6: Effects of (a) membrane regularization on W_C^m for different element sizes and (b) bending regularization for $l_e/t_e = 1$. Note that the final CL failure parameter used in the simulation for pure bending is independent of the element size.

5 Component tests

Three-point bend tests of notched steel beams were conducted to evaluate the material model on a load case that was not used in the calibration procedure. Figure 7 shows the geometry that consists of a hat profile which is spot welded to a bottom plate. A total of 36 spotwelds were used for each component.

Steel cylinders with a diameter of 60 mm were used as both punch and supports. We inserted Teflon sheets between the profile and the supports and punch to minimize the effects of friction (Figure 7(b)). By measuring the displacement of various points on the punch and profile we could find the punch displacement that was unpoluted by the compliance of the Teflon sheet.

The punch was centered over the notch and the distance between the supports was 340 mm. The tests were conducted in an Instron 5982 (100 kN) test machine at a loading speed of 5 mm/min.

Figure 8(a) shows the force-displacement curves from the five test repetitions, and (b) shows images taken just before and after fracture. The peak force of approximately 16 kN occurs at a punch displacement of about 8.5 mm in all the tests. Fracture takes place at a punch displacement between 24 mm and 27 mm.

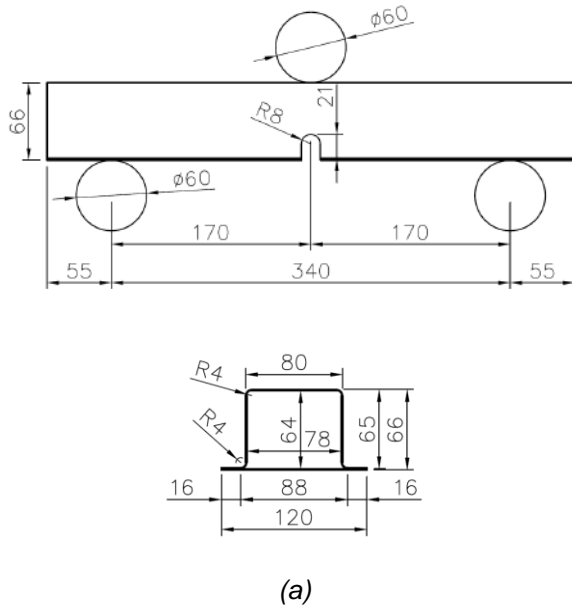


Figure 7: Three-point bend test. (a) Plan and cross section geometry. (b) Overview of the test setup.

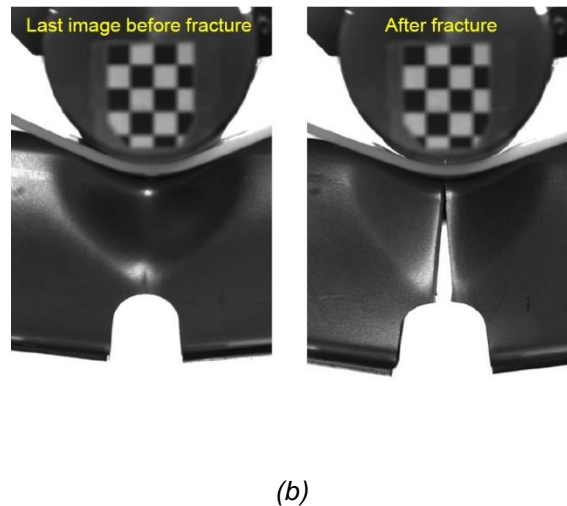
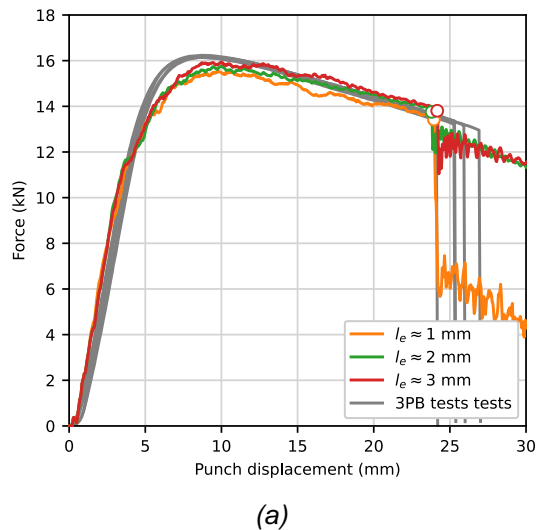


Figure 8: (a) Three-point bend test results compared to shell element simulations. (b) Representative images from a test.

6 Model evaluation

To evaluate the performance of ***MAT_258** with the ECL fracture surface we made shell finite element models of the three-point bend test presented in Section 5. We used element side-lengths of 1.0 mm, 2.0 mm, and 3.0 mm to challenge the regularization approach. Since the thickness of the plate is 1.0 mm, these element side lengths correspond to length-to-thickness ratios (l_e/t_e) of 1.0, 2.0 and 3.0. We used **ELFORM = 2** with five integration points over the thickness and an hourglass control type **IHQ = 4** with **QM = 0.03**. A general contact algorithm ***CONTACT_AUTOMATIC_SINGLE_SURFACE** with **SOFT = 1** and **VDC = 20** was used along with a friction coefficient of 0.1. On the ***CONTROL_SHELL** card we used **ISTUPD = 1**, **BWC = 1**, **PROJ = 1**, and **IRNXX = -2**. In ***MAT_258**, element erosion occurs when 40% of the through-thickness integration points reach its failure criterion.

In general, Figure 8(a) shows that the correspondence between the simulations and the experiments is good. Also, the regularization procedure works as intended. The displacement at the first instance of fracture is 24 mm for all the simulations which is just inside the lower bound of the experimental scatter. In the experiments, the crack propagated very quickly from the notch root towards the punch. Due to the size of the finite elements, the crack is significantly blunter in the simulations and the crack growth in the simulations is not as quick as in the tests.

The images in Figure 9 from a simulation with $l_e/t_e = 1$ illustrate the last frame before fracture. The damage parameter is shown in (a) where we see that the fracture initiates in the notch root, just as in the test. Damage values of approximately 0.25 occur near the punch. Figure 9(b) shows the bending indicator Ω . While the material directly below the punch experiences almost pure bending (Ω close to 1) throughout the simulation, the material in the notch root experiences almost pure membrane loading and Ω is generally below 0.1.

A list of history variables for ***MAT_258** can be found in Holmen et al. [6].

One significant advantage of the bending regularization scheme is that segments of the profile that are heavily strained due to bending, will not suffer premature failure with small elements, which can be a problem without such bending regularization.

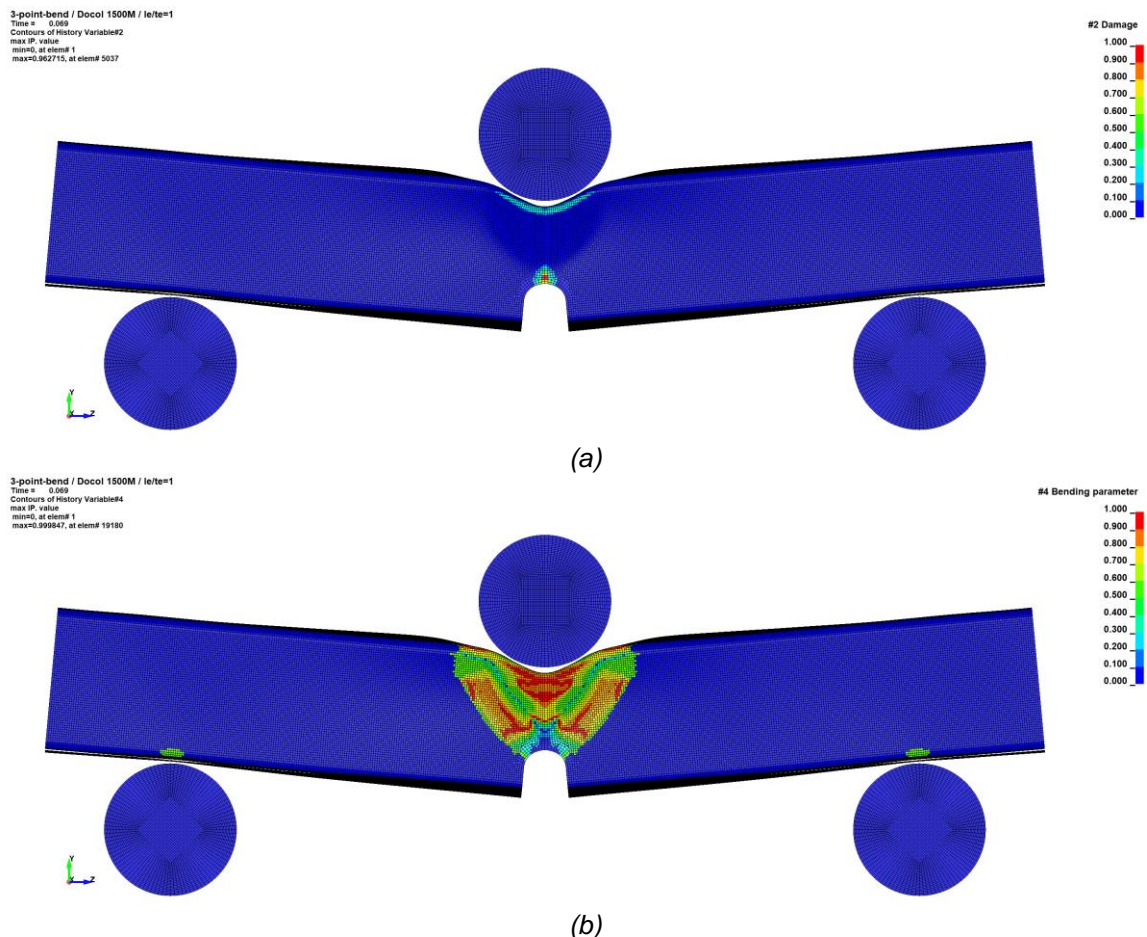


Figure 9: Screenshots from the last simulation frame before fracture. (a) Damage parameter. (b) Bending indicator.

Summary

This paper presents the necessary steps to calibrate *MAT_258 with a Lode dependent Extended Cockcroft-Latham (ECL) fracture surface. Three material tests with corresponding solid element simulations are required for calibration. Three-point bend tests were applied to evaluate the performance of the model. The results are satisfactory for three different element sizes as the occurrence of the first fracture is predicted within the experimental scatter.

Acknowledgment

The work was conducted when JKH and JJ were full-time employees at NTNU. Funding came from the Research Council of Norway through the FORNY2020 program. The project was carried out with help from Hydro Extruded Solutions, Audi, and Dynamore Nordic. We would like to acknowledge SSAB for providing the steel plates that were used for the part of the project pertaining to this document.

References

- [1] Kõrgesaar M, Remes H, Romanoff J: "Size dependent response of large shell elements under in-plane tensile loading", International Journal of Solids and Structures 51, 2014, 3752-3761.
- [2] Pack K, Mohr D: "Combined necking & fracture model to predict ductile failure with shell finite elements", Engineering Fracture Mechanics 182, 2017, 32-51.
- [3] Andrade FXC, Feucht M, Haufe A, Neukamm F: "An incremental stress state dependent damage model for ductile failure prediction", International Journal of Fracture 200, 2016, 127-150.
- [4] LS-DYNA Keyword User's Manual. Volume II: Material Models. LS-DYNA R12 09/08/2020.
- [5] Costas M, Morin D, Hopperstad OS, Børvik T, Langseth M: "A through-thickness damage regularisation scheme for shell elements subjected to severe bending and membrane deformations", Journal of the Mechanics and Physics of Solids 123, 2019, 190-206.
- [6] Holmen JK, Johnsen J, Morin D, Børvik T, Langseth M: "Application of *MAT_258 for Bending and Crushing of Extruded Aluminum Profiles Using Shell Elements", 16th International LS-DYNA Conference, 2020, 1-13.
- [7] Johnsen, J., Holmen, J.K, Gruben, G., Morin, D., T., Langseth, M.: "Calibration and Application of GISSMO and *MAT_258 for Simulations Using Large Shell Elements", 16th International LS-DYNA Conference, 2020, 1-16.
- [8] Wierzbicki T, Bai Y: "A new model of metal plasticity and fracture with pressure and Lode dependence", International Journal of Plasticity 24, 2008, 1071-1096.
- [9] Gruben G, Hopperstad OS, Børvik T. "Evaluation of uncoupled ductile fracture criteria for the dual-phase steel Docol 600DL", International Journal of Mechanical Sciences 62, 2012, 133-146.
- [10] Grimsmo EL, Aalberg A, Langseth M, Clausen AH. "Failure modes of bolt and nut assemblies under tensile loading", Journal of Constructional Steel Research 126, 2016, 15-25.
- [11] Børvik T, Hopperstad OS, Berstad T, Langseth M. "A computational model of viscoplasticity and ductile damage for impact and penetration", European Journal of Mechanics – A/Solids 20, 2001, 685-712.
- [12] <https://www.ntnu.edu/kt/ecorr> [accessed 13.08.2021]